JOURNAL OF MATERIALS SCIENCE 25 (1990) 4644-4653

Tensile strength of discontinuous fibre-reinforced composites

Y. TERMONIA
Central Research and Development Experimental Station, E.I. du Pont de Nemours, Inc., Wilmington, Delaware 19898, USA

A stochastic Monte-Carlo approach, based on Eyring's chemical activation rate theory, is used to study the factors controlling the tensile strength of discontinuous fibre-reinforced composites. The model explicitly takes into account the local distribution of stress near fibre ends. Both the fibre and the matrix are allowed to break during fracture of the composite. The stress–strain curves and the modes of failure of the composite are found to be strongly dependent on the volume fraction and aspect ratio of the fibres. The importance of adhesion at the fibre/matrix interface is also studied. The results are compared with available experimental data.

1. Introduction

Composites made by embedding stiff fibres in soft matrices can have outstanding mechanical properties, encompassing the advantages of both the fibre and the matrix, i.e. high strength and high elongation at break. For better processability, these composite materials often incorporate short discontinuous fibres which, ideally, are also oriented in the direction of applied load in order to take full advantage of the reinforcing properties of the fibres.

Several theoretical, as well as empirical, "combining rules" have been developed for predicting the dependence of the composite stiffness on the concentration and the known mechanical properties of the individual components (for a review, [1]). Similar combining rules have been developed in theoretical studies of composite strength [2–4]. All the above approaches, however, are usually based on the so-called shear analysis and therefore neglect the stressed state of the fibre ends. That neglect is probably of secondary importance in calculations of the composite stiffness at small deformations. However, in the case of large deformations approaching failure, the stress concentration near fibre ends becomes of crucial importance. As a result, analytical equations for describing composite strength are far from being as accurate and rigorous as those introduced for describing composite stiffness. For that reason, finite element analyses involving a detailed calculation of internal stresses have also been used [5]. These studies, however, were restricted to the case of particulate composites and they also neglected the effects of particle–particle interactions. In addition, a very simplified criterion was used for predicting composite failure.

In a recent series of publications [6, 7], we have introduced a finite difference type of approach for the study of the factors controlling the stiffness of fibre-reinforced composites. The approach is especially well-suited for application to composite strength because it explicitly takes into account all local stress concentration effects. In the model, the composite material is represented by a three-dimensional lattice of bonds having different elastic constants for the fibre and for the matrix. For a given value of the external strain, the lattice sites are relaxed towards mechanical equilibrium with their neighbours by a systematic sequence of operations which steadily reduce the net residual force acting on each site. That model is extended here to a study of composite strength by use of a stochastic approach previously introduced for describing polymer failure [8–10]. Within the framework of that approach, the lattice bonds are broken according to their local stress with the help of a Monte-Carlo lottery based on Eyring's chemical activation rate theory [11]. Bonds belonging to both the fibre and the matrix are allowed to break during fracture of the composite.

The model described above is used to study the dependence of composite strength on the volume fraction and aspect ratio of the fibres. The shape of the stress–strain curves and the mode of composite failure are found to be strongly dependent on fibre characteristics. The importance of adhesion at the fibre–matrix interface is also discussed.

2. The model

The composite is represented by a three-dimensional (x–y–z) lattice of sites which are linked by bonds having different elastic constants for the matrix and the fibre (for more details, see [6, 7]). The lattice is of the simple cubic type and typically comprises 200 nodes along the y-axis and 35 nodes in the transverse x- and z-directions. The Young and shear moduli of the matrix and of the fibre are denoted by (E_m, G_m) and (E_f, G_f), respectively. The fibres are oriented along the y-axis and have an aspect ratio l/d where l and d are length and diameter, respectively. In most simulations, d is set equal to 3 to 5 lattice units [6, 7].

0022–2461/90 $03.00 + .12

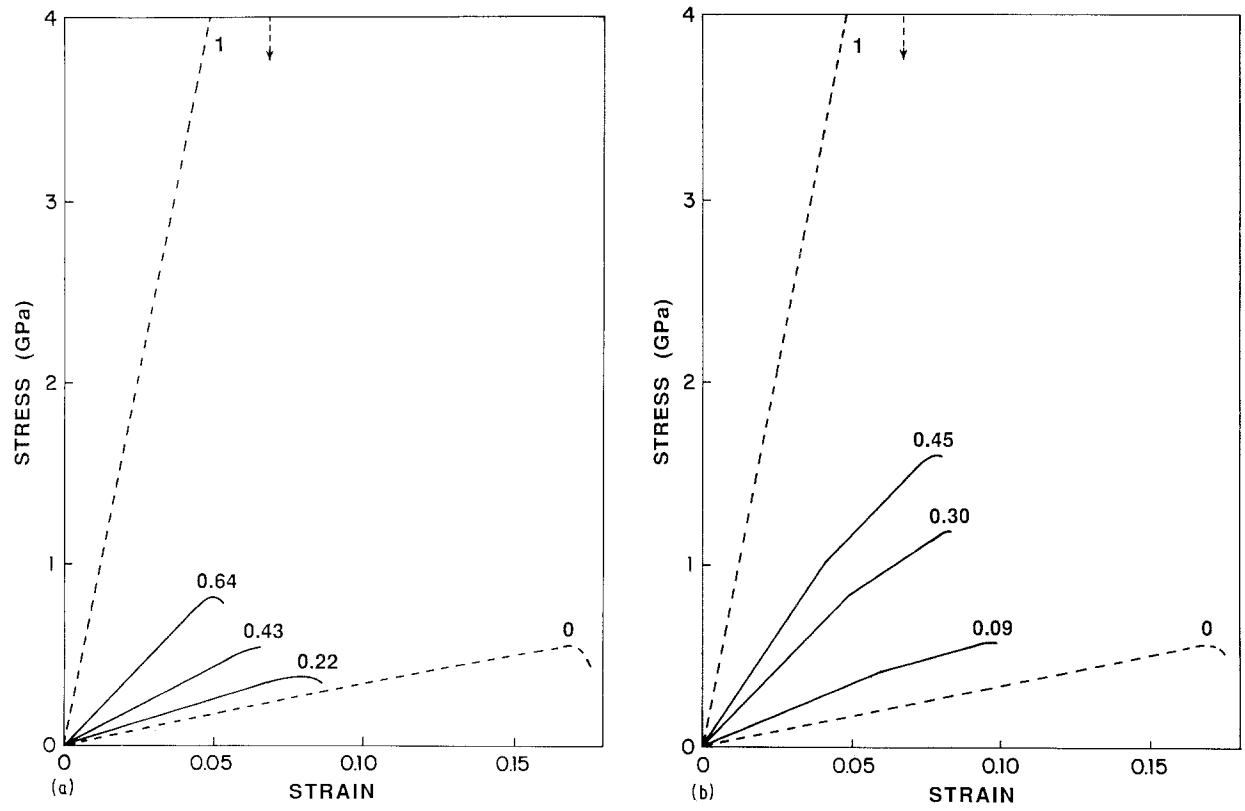

Figure 1 Stress–strain curves for a fibre-reinforced composite at different values of fibre volume fraction, v_f. (a) $l/d = 1$ with $d = 7$ lattice units; (b): $l/d = 20$ with $d = 1$ lattice unit. The dashed lines indicate the limiting cases of pure fibre ($v_f = 1$) and pure matrix ($v_f = 0$).

The lattice described above is strained along the y-axis at a constant rate of deformation and temperature, T. In the course of that process, bonds are broken according to the kinetic theory of fracture [11], i.e. at a rate

$$v = \tau \exp [(-U + \beta\sigma)/kT] \quad (1)$$

in which U is the activation energy, τ the thermal vibration frequency ($\sim 10^{12}$ sec^{-1}) and β an activation volume. In Equation 1, σ is the local stress

$$\sigma = K\varepsilon \quad (2)$$

where K is the elastic constant for the bond whereas ε is its local strain. That bond breaking process is executed with the help of a Monte-Carlo process (for more details, see [8–10]) which, at regular time intervals, also relaxes the lattice to its minimum energy configuration. That relaxation procedure leads, for each lattice site, to motions along the coordinate axes. For simplicity, these motions are assumed to be mutually independent and we focus on displacements along the y-axis along which the composite is strained. Thus the strain values, ε (see Equation 2), are for elongations along the y-axis and they represent either an axial tensile strain (for bonds along the y-axis) or a shear strain (for bonds along the transverse x- and z-axes). Similarly, K in Equation 2 denotes a tensile modulus (E_m or E_f) or a shear modulus (G_m or G_f).

Application of the model described above requires a detailed knowledge of the values for the activation energies, U, and activation volumes, β (Equation 1), for the various types of bonds. These sets of values are rather difficult to determine experimentally. At any rate, a quantitative description of the mechanical properties of a particular composite is beyond the scope of the present work. Therefore, for simplicity, we assume a hypothetical situation in which both the fibre and the matrix are isotropic so that U and β are the same for all the bonds belonging to the same component. Values of U and β for a given component (matrix or fibre) are then selected so as to give reasonable values for its tenacity and elongation at break. Typical parameter values are as follows.

Testing conditions: the temperature is set equal to 23° C and the rate of elongation $= 1\,\text{min}^{-1}$.

Fibre: we choose $U = 50\,\text{kcal mol}^{-1}$, $\beta = (0.331\,\text{nm})^3$ and $E_f = 80\,\text{GPa}$. The fibre is assumed to have an infinite molecular weight and to be therefore defect-free (cf. [8, 9]). The above parameter values lead (at the selected testing conditions) to an elongation at break around 6% and a tenacity of 5.6 GPa. Poisson's ratio for the fibre is set equal to $\nu_f = 0.25$ so that $G_f = 26\,\text{GPa}$.

Matrix: we take $U = 29\,\text{kcal mol}^{-1}$, $\beta = (0.49\,\text{nm})^3$ and $E_m = 3.3\,\text{GPa}$. This gives an elongation and tenacity at break of 17% and 0.56 GPa, respectively. Taking $\nu_m = 0.50$ for the matrix leads to $G_m = 1.1\,\text{GPa}$.

The above parameter values thus describe the case of composites made of stiff brittle fibres embedded in ductile and soft matrices, a situation which is most commonly encountered experimentally.

3. Results and discussion

Fig. 1a shows a series of stress–strain curves for a fibre-reinforced composite with $l/d = 1$, at different values of the fibre volume fraction, v_f. The curves for the pure matrix ($v_f = 0$) and for the pure fibre ($v_f = 1$) are denoted by dashed lines. Inspection of the curves shows that the additon to the matrix of stiff

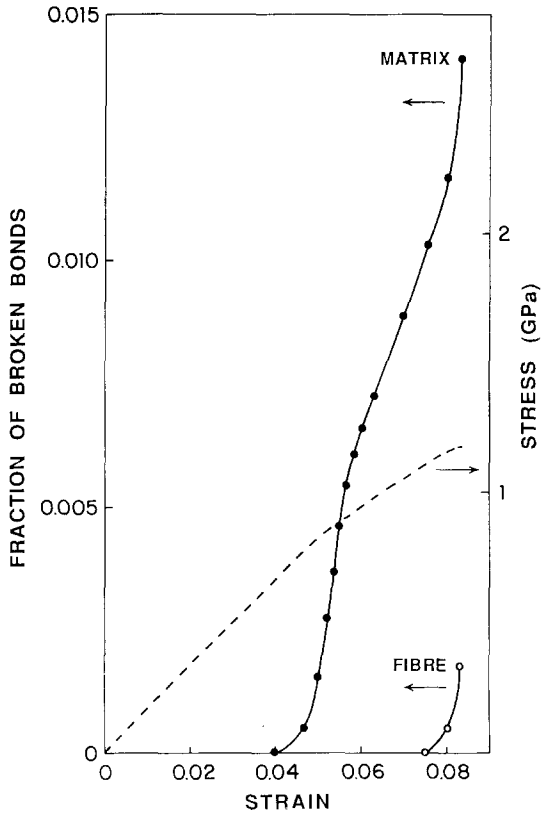

Figure 2 Dependence on strain of the fraction of broken matrix (●) and fibre (○) bonds. The fraction for a given component (fibre or matrix) is in units of the total number of bonds for that component. The figure is for a lattice of 19 × 19 × 300 bonds with $l/d = 20$, $d = 1$ and $v_f = 0.3$. The corresponding stress–strain curve is also represented (dashed line) for easy reference.

fibre particulates produces two effects: an increase in modulus and a decrease in the strain at break. These two effects have opposing influences on the tenacity and can lead, at low $v_f < 0.4$, to a composite strength lower than that for the pure matrix. Further investigation shows that fracture of the composite is initiated through tensile failure of the matrix near fibre ends. As $l/d = 1$, the concentration of those fibre ends is high and the local cracks therefore quickly merge transversely from the direction of applied load. Catastrophic failure of the composite then occurs with no breaking of the fibres (except at high $v_f \gg 0.5$).

The case of fibres with higher aspect ratio ($l/d = 20$) is described in Fig. 1b. Here, each stress–strain curve shows the presence of two distinct regions characterized by different moduli. We note that similar curves have been obtained experimentally by Curtis *et al.* [12] for a polyamide thermoplastic reinforced with glass and carbon fibres. The first region in Fig. 1b exhibits features that closely resemble those observed for $l/d = 1$ (see above). Inspection of the computer results indeed reveals that, as for the case of particulates, termination of that first region occurs through tensile failure of the matrix at fibre ends. Also, as in Fig. 1a, that termination is seen to occur at a strain value which decreases with v_f because the higher v_f, the higher the concentration of fibre ends. However, in contrast to the case of Fig. 1a, growing matrix cracks at fibre ends are quickly blunted by neighbouring fibres and no catastrophic failure occurs. Further straining of the composite then occurs at a lower modulus which is characteristic of the second region of the stress–strain curves in Fig. 1b. A detailed analysis of the computer results for that region (see Fig. 2) reveals further growth of those local matrix cracks and a gradual transfer of load to the neighbouring fibres. (Note that the modulus does not decrease appreciably within that second region, even though the matrix shows a continuous degradation (see Fig. 2). The reason for that constancy in modulus is the gradually increasing role of the fibres which are much stiffer than the surrounding matrix. That constancy is at variance with the steady decrease in modulus observed experimentally by Curtis *et al.* [12]. The reason for that discrepancy could be due to the fact that the fibres in [12] were not oriented so that their stiffness along the tensile axis is rather low.) Catastrophic failure of the composite then occurs when the stress supported by the fibres exceeds their maximum tensile strength. Note that the strain at break decreases with v_f, in accordance with the experimental data of Curtis *et al.* [12].

The discussion presented above is more clearly exemplified by Fig. 2 which depicts the dependence on strain of the fraction of broken matrix and fibre bonds for $l/d = 20$ and $v_f = 0.30$. The corresponding stress–strain curve is also represented (dashed line) for easy reference. The figure shows a progressive matrix failure, starting near 4 to 5% strain at which the first region terminates. For the present case of perfect adhesion between fibre and matrix, that failure occurs only in tension with no fibre debonding being observed. Fibre fracture is initiated near 8% strain, leading to catastrophic failure of the composite. The results of Fig. 2 bear a striking resemblance to the acoustic emission results of Curtis *et al.* [12]. The latter indeed show an acoustic output commencing at the end of the first region and accelerating rapidly with increasing composite strain. That output has been attributed to matrix cracking at fibre ends with fibre breakage occurring only near catastrophic failure of the sample [12].

The various modes of fracture for $l/d = 20$, discussed above, are further illustrated in Fig. 3. The figure show two successive deformation schemes obtained in a longitudinal x–y plane passing through the centre of the lattice. Fig. 3a, typical of the end of the first region in the stress–strain curve, clearly illustrates the tensile failure of the matrix near the fibre ends. Further straining of the composite leads to transverse propagation of those matrix cracks with eventual fibre breaking near catastrophic failure (Fig. 3b). These figures should be contrasted to those obtained for the case of particulate-reinforced composites ($l/d = 1$, Figs 3c, d). Here, the local matrix cracks appearing at "fibre" ends (Fig. 3c) easily merge transversely and catastrophic failure of the composite occurs with no "fibre" fracture being observed (Fig. 3d).

We now turn to a study of the dependence of composite strength on v_f and l/d. Previous phenomenological theories (see, for example, [2]) lead to the prediction that, at very small v_f, the strength, σ, should decrease as $\sigma = \sigma_m(1 - v_f)$ (see dotted line b

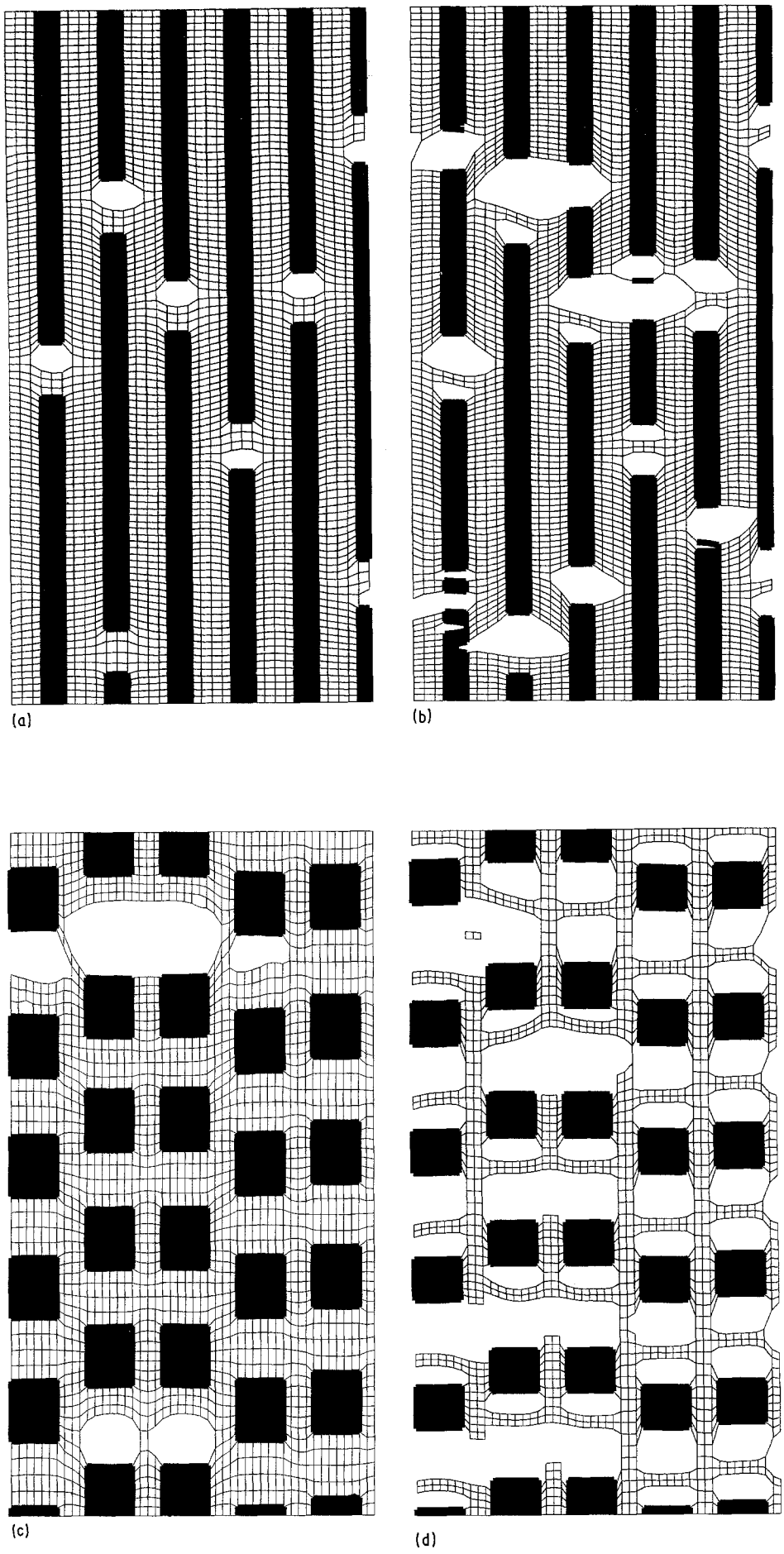

Figure 3(a), (b) Typical deformation schemes obtained for $l/d = 20$ ($d = 3$ and $v_f = 0.46$) at two different strain values, ε: (a) $\varepsilon = 0.035$ (end of first region in fig. 1b), (b) $\varepsilon = 0.075$ (near catastrophic failure). Perfect adhesion at the fibre–matrix interface is assumed. The figure is for a longitudinal x–y plane passing through the centre of the lattice. The x and y axes are not to scale. (c), (d) Typical deformation schemes obtained for $l/d = 1$ ($d = 7$ and $v_f = 0.37$) at two different strain values, ε: (c) $\varepsilon = 0.065$, (d) $\varepsilon = 0.085$ (near catastrophic failure). Perfect adhesion at the fibre–matrix interface is assumed. The figure is for a longitudinal x–y plane passing through the centre of the lattice. The x and y axes are not to scale.

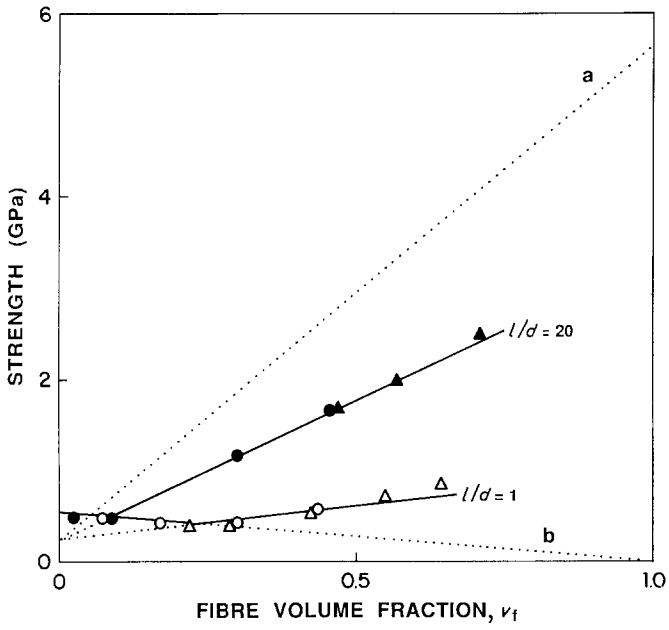

Figure 4 Dependence of tensile strength on fibre volume fraction, v_f. (●) $l/d = 20$ ($d = 1$); (▲) $l/d = 20$ ($d = 3$); (○) $l/d = 1$ ($d = 3$); (△) $l/d = 1$ ($d = 7$). The dotted lines a and b extending across the graph represent the following equations: a, $\sigma = \sigma_f v_f + \sigma_m^*(1 - v_f)$; b, $\sigma = \sigma_m(1 - v_f)$ in which $\sigma_f = 5.6\,\text{GPa}$, $\sigma_m^* = 0.23\,\text{GPa}$ and $\sigma_m = 0.56\,\text{GPa}$.

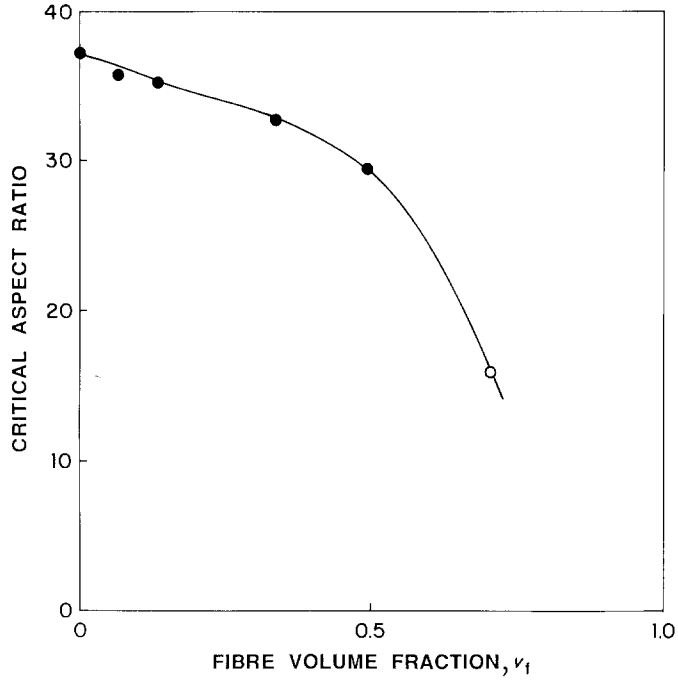

Figure 5 Dependence of critical aspect ratio on fibre volume fraction, v_f. Very long fibres with $l/d = 100$ were used in the calculations. (●) $l = 100$, $d = 1$ with lattice of $19 \times 19 \times 320$ sites; (○) $l = 300$, $d = 3$ with lattice of $10 \times 10 \times 1000$ sites.

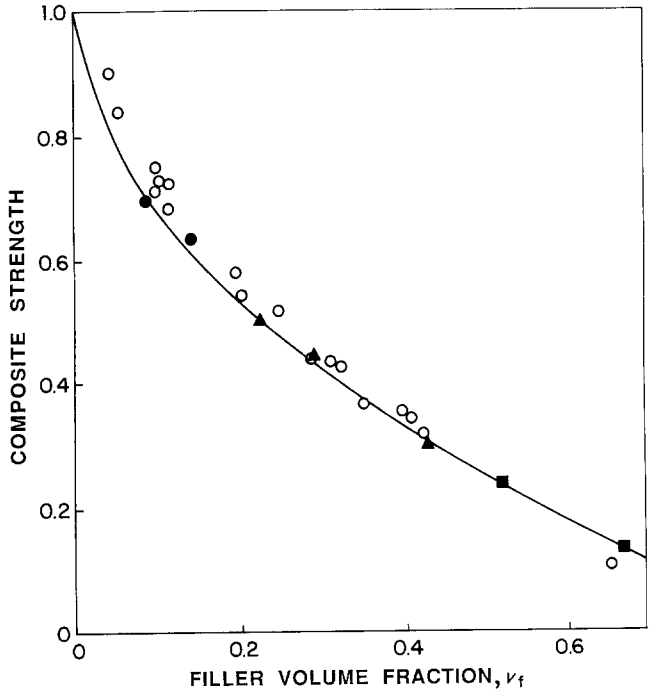

Figure 6 Dependence of composite strength on filler volume fraction, v_f, for the case of spherical particles with no adhesion to the matrix. The composite strength is in units of the strength of the pure matrix. (○) Experimental data for six composite materials taken from [16]. Solid symbols connected by the continuous line are predictions of the model for $l/d = 1$ with (●) $d = 5$, (▲) $d = 7$ and (■) $d = 9$.

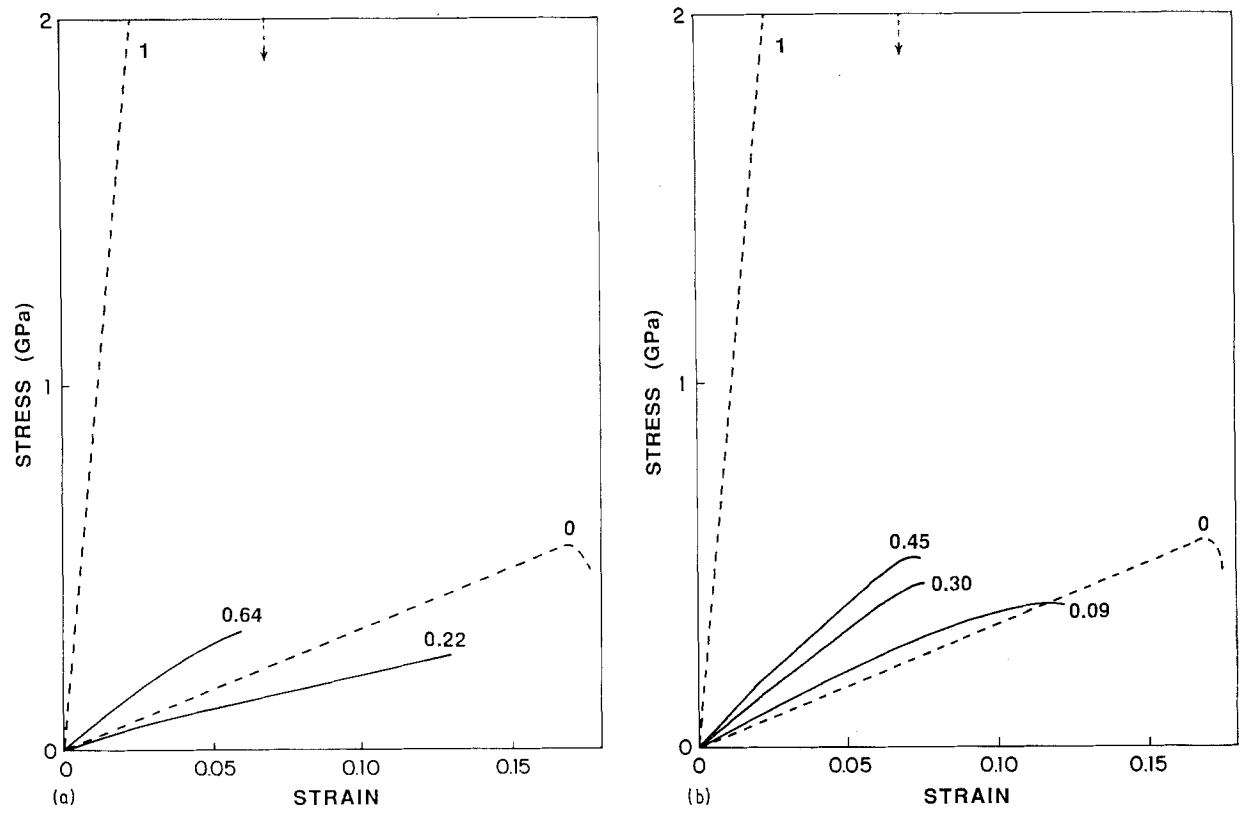

Figure 7 Stress–strain curves for a fibre-reinforced composite with poor adhesion, at different values of the fibre volume fraction, v_f. The adhesion factor was set equal to 0.1. (a) $l/d = 1$ with $d = 7$ lattice units; (b) $l/d = 20$ with $d = 1$ lattice unit. The dashed lines indicate the limiting cases of pure fibre ($v_f = 1$) and pure matrix ($v_f = 0$).

in Fig. 4) in which $\sigma_m (= 0.56\,\text{GPa})$ is the strength of the pure matrix. At higher v_f, a crossover is expected to $\sigma = \sigma_f v_f + \sigma_m^*(1 - v_f)$ (see dotted line a in Fig. 4) where σ_f (= 5.6 GPa) is the strength of the pure fibre, whereas σ_m^* (= 0.23 GPa) is the stress on the matrix at the breaking strain of the fibre. These predictions, however, are valid only for the case of continuous fibres assuming an isostrain situation within the composite. The case of discontinuous fibres is much more complex because it requires a detailed knowledge of the stress concentration near fibre ends. The problem is thus ideally suited for analysis with the help of our approach. Our results for $l/d = 20$ (solid symbols) and $l/d = 1$ (open symbols) are presented in Fig. 4 and compared to the predictions of lines a and b. The data follow two different regimes, depending on the fibre volume fraction. At low v_f, our strength values follow line b, therefore indicating that the fibres play no major role and the strength is matrix dominated. At a critical v_f whose value decreases with l/d, a second regime appears in which the tenacity becomes fibre dominated. Tenacity now increases with v_f and the data follow a series of lines all originating at $\sigma_m^* =$ 0.23 GPa and roughly linear with a slope increasing with l/d. These lines are very similar to line a, which represents their limiting behaviour for $l/d = \infty$. Note also that all our strength values for a given l/d are independent of our choice of the value (in lattice units) for the fibre diameter. This stresses confidence that our results are independent of model details.

The actual values of the slopes in the second regime in Fig. 4 are determined by the ratio of l/d over the

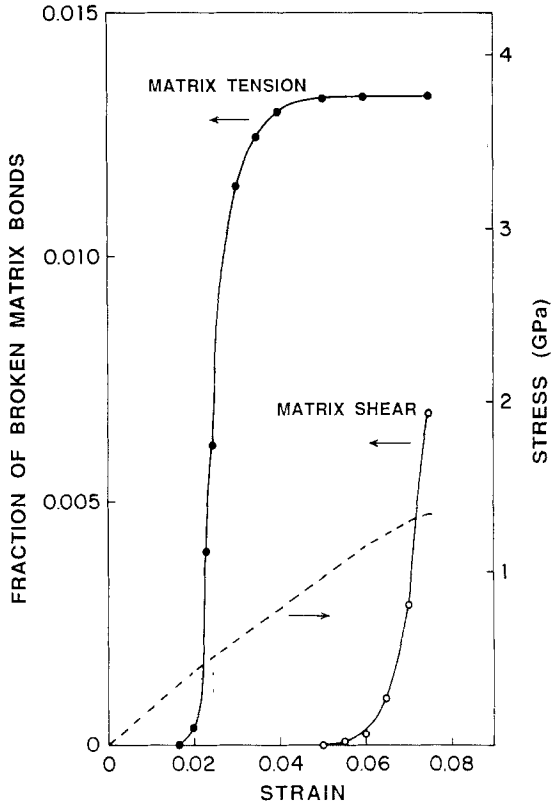

Figure 8 Dependence on strain of the fraction of broken matrix bonds for the case of poor adhesion. The fraction is decomposed into two contributions: failure (●) in tension and (○) in shear. The figure is for a lattice of 19 × 19 × 300 bonds with $l/d = 20$, $d = 1$, $v_f = 0.3$ and an adhesion factor equal to 0.1. The corresponding stress–strain curve is also represented (dashed line) for easy reference.

critical aspect ratio which is required for an efficient transfer of load from the matrix to the fibres [2, 6, 7]. That critical aspect ratio, l_c/d, is known to be a strong function of the ratio of elastic moduli between fibre and matrix [6]. Fig. 5 shows that the l_c/d also depends on the fibre volume fraction, v_f. In the limit $v_f = 0$, we recover the result $l_c/d = 37$ obtained in [6,7] for the case of a single fibre embedded in an infinitely large matrix with $E_f/E_m = 24$. As v_f is increased from 0 to 0.5, that value of l_c/d stays rather constant and shows only a small drop from 37 to 30. At higher fibre content, however, l_c/d decreases sharply with fibre volume fraction towards the limiting value 0, expected at $v_f = 1$. That sharp decrease explains the faster than linear increase in strength with v_f observed in Fig. 4 for $v > 0.5$. The figure also shows that, the lower l/d, the faster and the more pronounced the non-linear increase in strength. Of course, at $v_f = 1$, all the curves in Fig. 4 are expected to converge towards the limiting value $\sigma_f = 5.6\,\text{GPa}$ for the pure fibre. Note, finally, that our dependence of l_c/d on v_f in Fig. 5 is much weaker than that predicted by Rosen [13] using the shear analysis method.

We now turn to a detailed study of the effect of adhesion at the fibre–matrix interface. Adhesion is one of the key factors determining the mechanical properties of fibre-reinforced composites. Previous theoretical models, however, tend to neglect the influence of the boundary layer of poor bonding developed between fibre and matrix during preparation of the composite. The importance of that so-called "mesophase" layer has been recognized recently [14] and its thickness has been estimated to be in the range 30 to 240 nm. Varying the adhesion in the model was realized by breaking bonds at the fibre–matrix interface with probability (1-adhesion factor). Unless otherwise specified, the interface of poor adhesion was assumed to have a thickness of one lattice unit.

The dependence of composite strength on v_f for the case of spherical inclusions ($l/d = 1$) with no adhesion to the matrix is studied in Fig. 6. The composite strength is in units of the strength of the pure matrix. Our results (continuous line connecting the filled-in symbols) show a sharp decrease in strength with an increase in filler content. That decrease follows the often conjectured relationship [15] $\sigma \approx (1 - \alpha v_f^{2/3})$ with $\alpha = 1.21$. Note that, again, our strength values are found to be rather independent of the particular value chosen for the particle diameter, d. Also represented in Fig. 6 are experimental data reported by Nicolais and Mashelkar [16] for six composite materials. A very good agreement with the theoretical predictions is found.

The effect of poor adhesion on the stress–strain curves for fibre-reinforced composites is studied in Fig. 7. The figure is qualitatively similar to Fig. 1 obtained for the case of good adhesion. Thus, again, the stress–strain curves for $l/d = 20$ (Fig. 7b) show the presence of two distinct regimes. Further investigation also shows that the mode of fracture for $l/d = 1$ is very similar to that observed for the case of good adhesion. Thus, cracks form in the matrix near fibre ends and easily propagate transversely, leading to catastrophic failure of the sample. The mode of failure for the case of long fibres ($l/d = 20$), however, strongly depends on the quality of adhesion at the fibre/matrix interface. A detailed analysis of the stress–strain curves in Fig. 7b reveals that the transition from the first to the second region is due to matrix cracking near fibre ends, as in Fig. 1b. However, in contrast to the case of good adhesion, transverse propagation of those cracks through tensile failure of the fibres does not occur. Rather, shear failure of the weak fibre/matrix interface is observed, leading to progressive fibre debonding. These results are clearly demonstrated in Fig. 8 for $v_f = 0.3$. Tensile fracture of the matrix near fibre ends starts near 2% strain and continues well into the second regime. Near 5% strain, the matrix starts to fail in shear, leading to a progressive debonding of the fibres. This initiates catastrophic failure of the composite, which occurs near 7.5% strain.

Two successive deformation schemes obtained for $l/d = 20$ with poor adhesion are represented in Figs 9a and b. At the end of the first region in the stress–strain curve, tensile failure of the matrix near fibre ends is the only mode of fracture being observed (Fig. 9a). Note the high concentration of stress building up at the fibre–matrix interface. Near catastrophic failure (Fig. 9b), the matrix starts to fail in shear and progressive debonding of the fibres is seen to occur. The case of particulates with poor adhesion is described in Figs 9c and d. Again, composite fracture is initiated through matrix failure at "fibre" ends (Fig. 9c). Because the concentration of "fibre" ends is high, these matrix cracks easily merge transversely, leading to catastrophic failure (Fig. 9c). No debonding, however, is seen to occur along the direction of applied load.

Our results for the dependence of composite strength on v_f and l/d for the case of poor adhesion are represented in Fig. 10. The notation and symbols are the same as for Fig. 4. At small v_f, our strength values decrease with fibre volume fraction therefore indicating that the mechanical properties of the composite are essentially matrix dominated. However, in contrast to the case of good adhesion (see Fig. 4), the data fall well below line b. Rather, they follow the dashed line c, obtained from Fig. 6, for the case of particulates with no adhesion to the matrix. At higher v_f, the tenacity becomes fibre dominated and increases with fibre volume fraction. For not too high $v_f < 0.5$, the data follow a series of straight lines originating at $\sigma_m^* = 0.23\,\text{GPa}$, as in the case of good adhesion (see previous Fig. 4). Note, however, that the slopes of those lines are much lower than those observed in Fig. 4. At $v_f > 0.5$, the critical length strongly decreases with fibre volume fraction (see Fig. 5 in that connection) and this results in a dramatic upsurge in tenacity.

Fig. 11 shows the dependence of composite strength on adhesion for an aspect ratio $l/d = 20$. The two sets of data are for different fibre volume fractions. Inspection of the figure shows that, the higher v_f, the more pronounced is the decrease in strength with adhesion. That decrease is seen to be particularly significant when the adhesion factor falls below 0.3 to 0.4. This

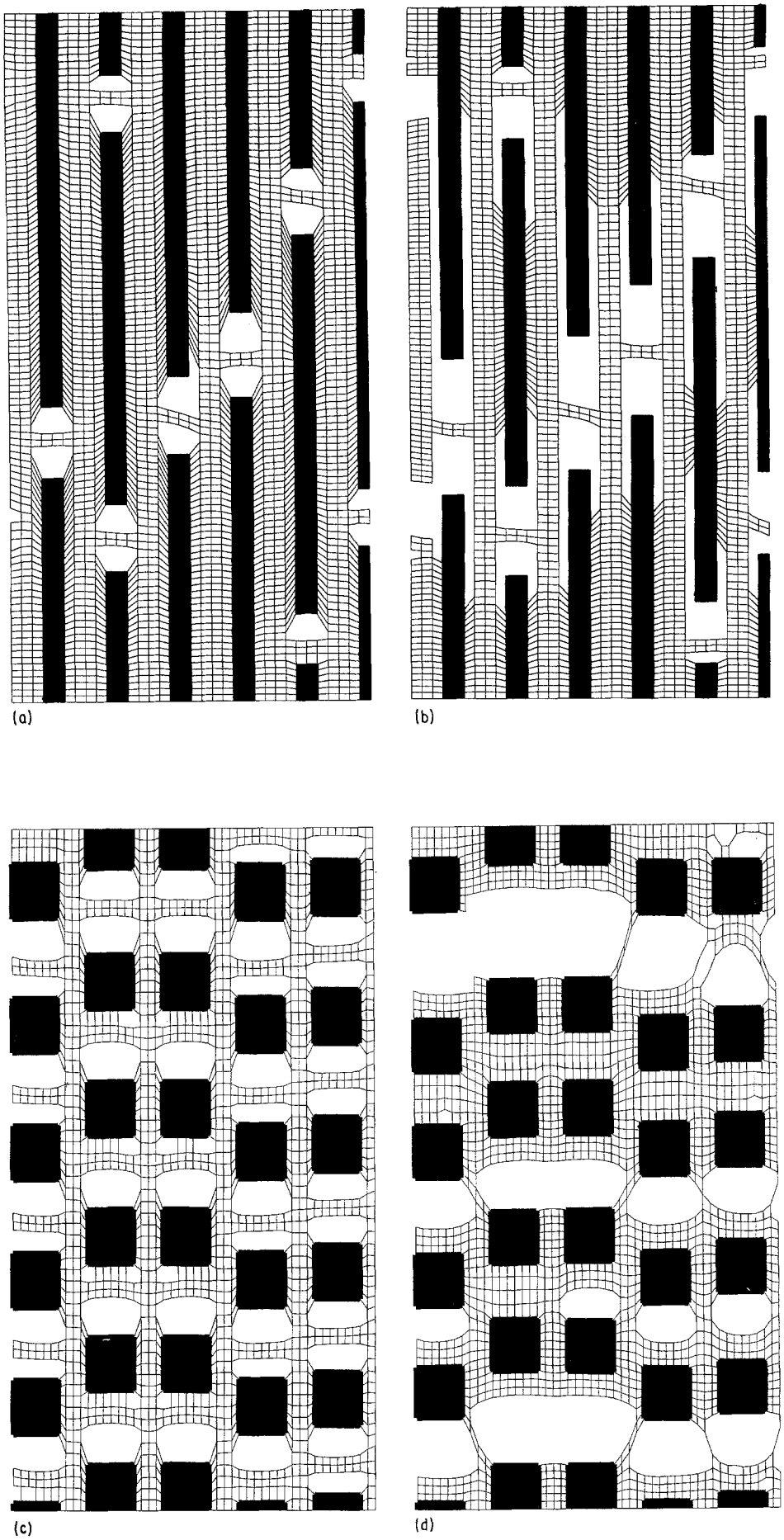

Figure 9(a), (b) Typical deformation schemes obtained for $l/d = 20$ ($d = 3$ and $v_f = 0.46$) at two different strain values, ε: (a) $\varepsilon = 0.025$ (end of first region in Fig. 7b), (b) $\varepsilon = 0.075$ (near catastrophic failure). An adhesion factor equal to 0.1 is assumed. The figure is for a longitudinal x–y plane passing through the centre of the lattice. The x and y axes are not to scale. (c), (d) Typical deformation schemes obtained for $l/d = 1$ ($d = 7$ and $v_f = 0.37$) at two different strain values, ε: (c) $\varepsilon = 0.08$, (d) $\varepsilon = 0.12$ (near catastrophic failure). An adhesion factor factor equal to 0.1 is assumed. The figure is for a longitudinal x–y plane passing through the centre of the lattice. The x and y axes are not on scale.

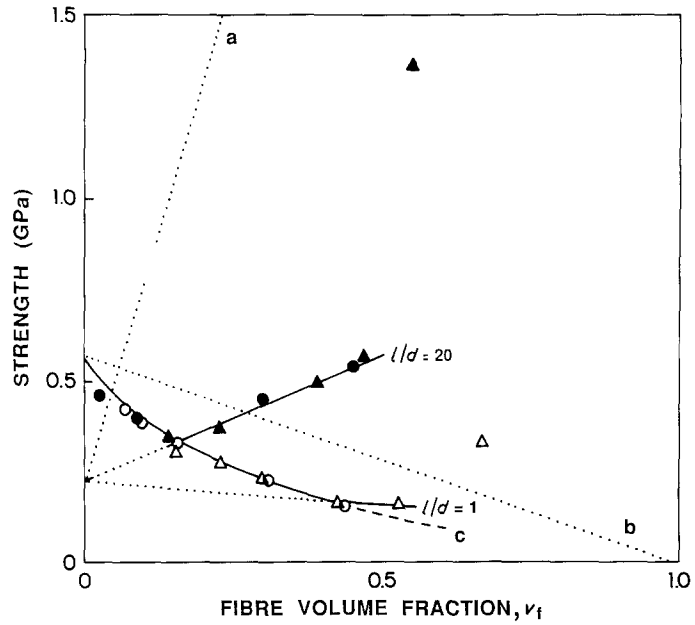

Figure 10 Dependence of tensile strength on fibre volume fraction, v_f, for the case of poor adhesion (adhesion factor = 0.1). (●) l/d = 20 (d = 1); (▲) l/d = 20 (d = 3); (○) l/d = 1 (d = 3); (△) l/d = 1 (d = 7). For details on the dotted lines a and b, see legend to Fig. 4. The dashed line c indicates the prediction of the continuous curve fitted to our data in Fig. 6.

result is in line with our previous observation (see [6, 7]) of a sharp increase in fibre critical length below 30% adhesion.

4. Conclusions

We have presented a new model for the description of the effects of adhesion and fibre characteristics on the strength of fibre-reinforced composites. The approach is microscopic in nature and allows detailed study of the interplay of fibre and matrix fracture during composite failure. The model also explicitly takes into account the importance of stress concentration near fibre ends and the redistribution of stress after local matrix or fibre failure.

A few comments should be devoted to the size of the "test sample" used in the calculations. As was mentioned earlier, a sample typically comprises 35 × 35 × 200 lattice sites. The fibre diameter is usually of the order of 3 to 5 lattice units which, for a 10 μm fibre, leads to a 2 to 3 μm distance between sites. From the above considerations, our sample thickness and length are of the order of 100 and 600 μm, respectively. The obvious question is whether the results of our calculations are affected by specimen size. It is well-known indeed, that composite strength is strongly affected by sample size as well as by fibre diameter, d (at constant l/d) [17]. As was mentioned in Section 3, however, our results are, as far as we could determine, independent of sample size and of the particular value chosen for d. This is not the case experimentally, because failure of actual composites is strongly dominated by gross flaws. In the absence of such flaws, as in the present model, no such effect is expected.

For simplicity, the present work focuses on composite deformation along the tensile y-axis and neglects lateral motions in the transverse x- and z-directions. This is an oversimplification without which the computer time required for the calculations would be prohibitively large. Thus, the model proposed may be too simple to describe fully the fracture behaviour of fibre-reinforced composites but, it brings out very clearly essential points like the role of fibre aspect ratio, fibre volume fraction and fibre/matrix adhesion. The present approach should be also very instructive

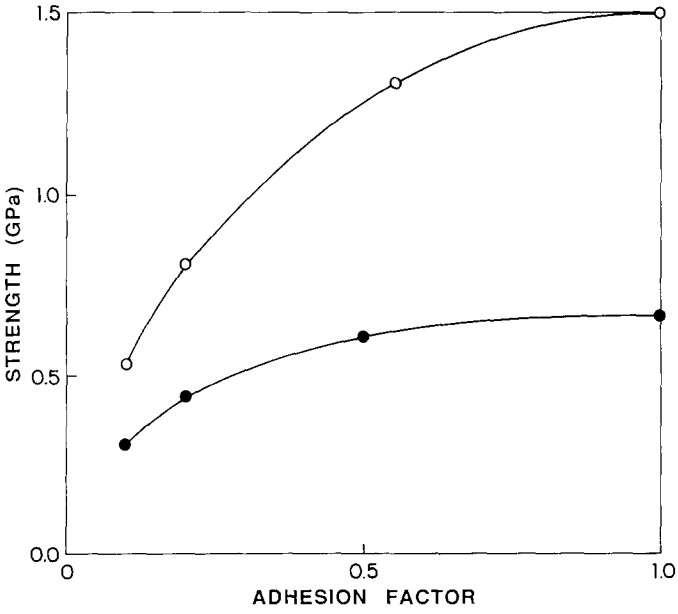

Figure 11 Dependence of tensile strength on adhesion factor at two different fibre volume fractions. The figure is for l/d = 20 with d = 3 lattice units. (○) v_f = 0.43; (●) v_f = 0.141.

in identifying additional key issues to be addressed in more advanced models.

References

1. A. A. BERLIN, S. A. VOLFSON, N. S. ENIKOLOPIAN and S. S. NEGMATOV, "Principles of Polymer Composites" (Springer-Verlag, Berlin, 1986).
2. A. KELLY, "Strong Solids" (Oxford University Press, Oxford, 1966).
3. J. R. VINSON and T. W. CHOU, "Composite Materials and their Use in Structures" (Elsevier Applied Science, Amsterdam, 1975).
4. J. YAMAKI, *J. Phys. D Appl. Phys.* **9** (1976) 115.
5. S. SAHU and L. J. BROUTMAN, *Polym. Engng Sci.* **12** (1972) 91.
6. Y. TERMONIA, *J. Mater. Sci.* **22** (1987) 504.
7. *Idem, ibid.* **22** (1987) 1733.
8. Y. TERMONIA, P. MEAKIN and P. SMITH, *Macromol.* **18** (1985) 2246.
9. *Idem, ibid.* **19** (1986) 154.
10. Y. TERMONIA and P. SMITH, *Polymer* **27** (1986) 1845.
11. H.-H. KAUSCH, "Polymer Fracture" (Springer-Verlag, Berlin, 1987).
12. P. T. CURTIS, M. G. BADER and J. E. BAILEY, *J. Mater. Sci.* **13** (1978) 377.
13. B. W. ROSEN *ASM* **72** (1965) 75.
14. P. S. THEOCARIS, *J. Appl. Polym. Sci.* **30** (1985) 621.
15. F. DANUSSO and G. TIEGHI, *Polymer* **27** (1986) 1385.
16. L. NICOLAIS and R. A. MASHELKAR, *J. Appl. Polym. Sci.* **20** (1976) 561.
17. G. LANDON, G. LEWIS and G. F. BODEN, *J. Mater. Sci.* **12** (1977) 1605.

Received 11 July
and accepted 21 November 1988